JOURNAL OF MATERIALS SCIENCE 8 (1973) 47–58

Anisotropy in the hardness and friction of calcium fluoride crystals

J. B. O'NEILL
Materials and Chemistry Department, Rolls Royce and Associates, Derby, UK

B. A. W. REDFERN
Material Science Section, British Railways Board, Derby, UK

C. A. BROOKES
Department of Engineering Science, University of Exeter, UK

Anisotropy in the Knoop indentation hardness and the friction of diamond cones on calcium fluoride crystals has been investigated at experimental temperatures from 20 to 300° C. It is shown that the directions of minimum and maximum indentation hardness, on the (001) plane, are ⟨110⟩ and ⟨100⟩ respectively whilst the ⟨1$\bar{1}$0⟩ are harder than the ⟨11$\bar{2}$⟩ directions on the (111) plane. Also, the sliding friction in the (001) plane is greatest in the ⟨110⟩ directions and least in the ⟨100⟩ and, on the (111) cleavage plane, [$\bar{1}\bar{1}$2] sliding leads to higher friction than [11$\bar{2}$]. The nature of anisotropy, for both hardness and friction measurements, does not change over the experimental temperature range covered in this work. Observations on the resultant deformation are made and these anisotropic properties are explained in terms of the effective resolved shear stresses developed on the {100} ⟨011⟩ primary slip systems at all experimental temperatures.

1. Introduction

The mechanical properties of ionic crystals are largely determined by limited plastic deformation, the formation of cracks due to dislocation interactions at low levels of strain and an intrinsic susceptibility to cleavage fracture. Many studies on crystals of the rocksalt structure, particularly magnesium oxide and lithium fluoride, have led to a greater understanding of dislocation behaviour in all crystalline solids. This work has been helped by the geometrical simplicity of the {110} ⟨1$\bar{1}$0⟩ primary slip systems and {100} cleavage. In recent years, anisotropy in the hardness and frictional properties of these crystals has been explained on the basis of bulk plastic deformation – even though much brittle fracture often accompanies the indentation or sliding mechanisms [1-5].

The mechanical properties of ionic calcium fluoride make an interesting comparison with those of the rocksalt structure. The fluorspar structure cleaves on {111} planes and, on the basis of compression experiments at elevated temperatures, the primary and secondary slip systems are believed to be {100} ⟨011⟩ and {110} ⟨1$\bar{1}$0⟩ respectively. [6]. In this paper we shall compare and contrast the behaviour of calcium fluoride, in hardness and friction measurements, with that of the rocksalt crystals. We shall also discuss the possibility of extending the earlier explanation for frictional anisotropy in magnesium oxide and lithium fluoride [2] to another ionic crystal which has different slip systems and cleavage characteristics.

2. Experimental details

Anisotropy in hardness was determined using the Knoop indenter in a Leitz Miniload hardness apparatus as described in an earlier paper [5]. In these experiments the hardness of a particular crystallographic direction, in a given crystal plane, is determined when the long diagonal of the indenter is coincident with that direction. Then the hardness value is calculated from the projected area of the indentation, based solely on the measurement of the long diagonal, divided into the normal load. Particular care was taken to ensure a constant time under load

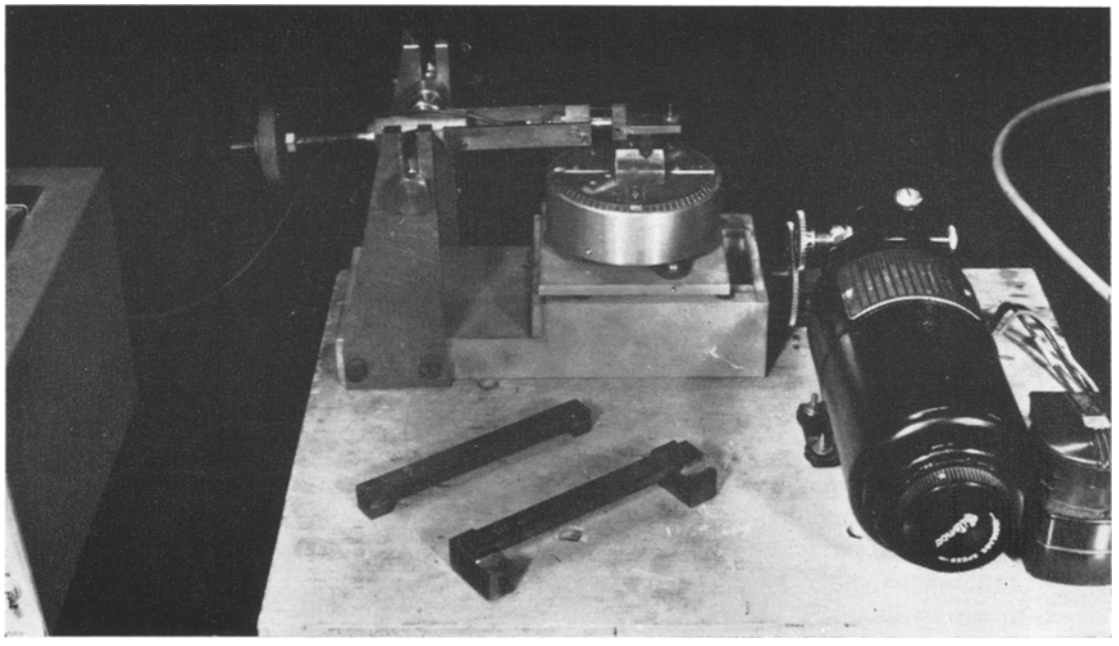

Figure 1 Photograph of the friction apparatus.

for hardness measurements made in those experiments designed to investigate anisotropy and the effect of temperature on the hardness of calcium fluoride. This was necessary because creep under a static indenter is significant in this material within the temperature range covered.

A photograph of the friction apparatus is shown in Fig. 1. The apparatus has been described in detail elsewhere [4] and only a brief description is given here. A slider was mounted on the end of a piezo-electric pressure transducer which was in turn attached to a counterbalanced pivoted bar. Normal loads were applied by the addition of weights directly on top of the slider and these weights were designed such that the centre of gravity of the loaded system was as near as possible to the cone tip. Horizontal specimens were clamped on a stage which could be rotated in increments of 5° from zero azimuth. The axis of rotation coincided with the vertical axis of the slider and the stage was mounted on a lathe traverse which could be moved parallel to the axis of the pressure transducer, by means of a variable speed electric motor, at speeds up to 20 mm min^{-1}. The resultant frictional forces placed the transducer in tension; the output was continuously amplified and fed into a pen recorder to give a permanent record of the friction over the length of a given track. Diamond sliders, in the form of cones with included angles of 60° and 90°, were used in these friction experiments.

Measurements of friction and hardness over a range of experimental temperatures from 20 to 300°C could be made, in specific low index crystallographic directions, when the rotating stage was replaced by a small hot plate on which the specimens were clamped. The specimen surface temperature was measured using a fine copper/constantan contact thermocouple.

The (111) surfaces of calcium fluoride were prepared by conventional cleavage techniques whilst (001) surfaces had to be prepared by mechanical polishing. Unfortunately, a suitable chemical polishing technique is not available for this material. Friction and hardness measurements were then made over the range of experimental temperatures given above. Optical microscopy, allied with dislocation etching using 0.4 N nitric acid for 45 min, was used to observe the nature of deformation associated with the friction and hardness measurements.

3. Results

3.1. Knoop hardness

Typical anisotropy in the hardness of (001) and (111) planes of calcium fluoride, using a 300 g normal load, is shown in Fig. 2. The effect on

hardness of increasing the experimental temperature, shown in Fig. 3, confirms that the hardness decreases uniformly for the low index directions on both planes and that there is little change in the anisotropy. Similarly, Fig. 4 shows that under conditions of creep and relaxation, i.e. maintaining the applied load for varying times at a constant experimental temperature, the behaviour of calcium fluoride is the same as that of other crystalline solids [7] and also that the nature of anisotropy is unchanged.

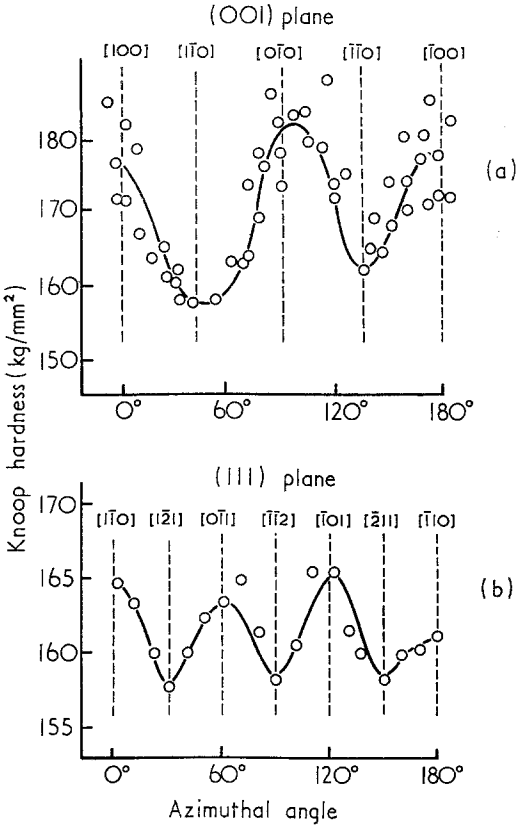

Figure 2 Anisotropy in hardness of calcium fluoride at 20°C on (a) the (001) plane and (b) the (111) plane.

3.2. Friction

Table I summarizes the effect of temperature on the coefficient of friction for the (001) and (111) planes of calcium fluoride in the important crystallographic directions. Three salient points emerge from a consideration of these results. First, the degree of anisotropy in friction becomes more pronounced with increasing experimental temperature – particularly on the (111) surfaces. Secondly, the high and low friction directions on

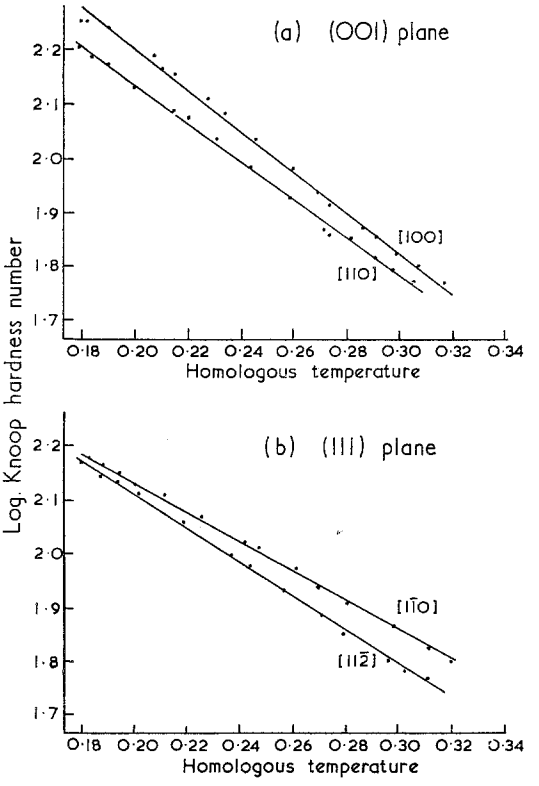

Figure 3 The effect of temperature on the hardness in principal crystallographic directions on (a) the (001) plane and (b) the (111) plane.

the cube planes, i.e. ⟨110⟩ and ⟨100⟩ respectively, are the converse of the anisotropy observed on similar planes of rocksalt crystals [2]. Finally, there is a marked degree of anisotropy on the (111) surface for sliding in the two different senses within the ⟨112⟩ family of crystallographic directions. A similar observation has been reported in studies on single crystal copper surfaces [8].

4. Deformation of the crystals

Indentations on the (001) plane of calcium fluoride are generally accompanied by a varying amount of predominantly sub-surface fracture. Comparable behaviour has been observed in hardness measurements on other crystals and is not thought to have any significant effect on the hardness values [5]. These cracks are probably produced after the indentation has been formed and when the material elastically recovers whilst the normal load is being removed. Photographs of typical indentations in [1$\bar{2}$1] and [1$\bar{1}$0] directions on a (111) cleavage plane are repro-

TABLE I

(001)			(111)				Slider and load
Temp.	[100]	[110]	Temp.	[112]	[112]	[110]	
22°C	0.62	0.64	20°C	0.67	0.78	0.72	
117°C	0.65	0.71	72°C	0.61	0.80	—	90° cone and 400 g load
233°C	0.70	0.75	133°C	0.54	0.89	—	
			253°C	0.54	1.01	—	
			300°C	0.83	1.22	—	60° cone and 1000 g load

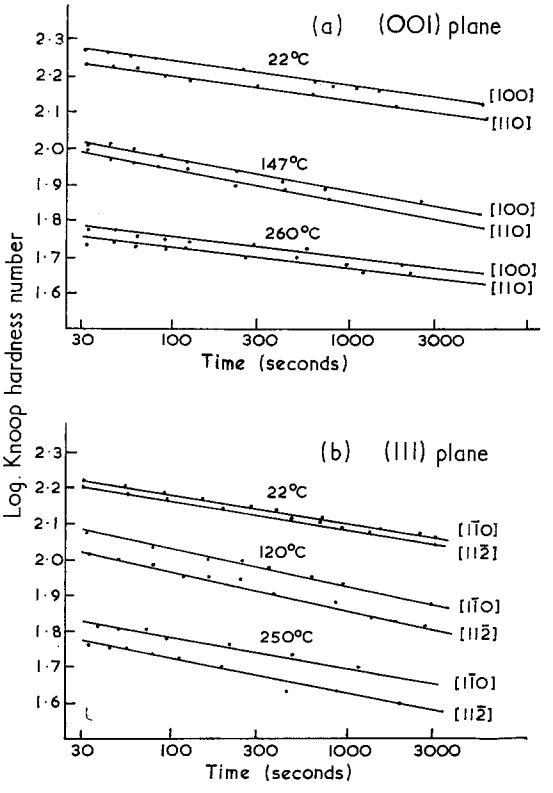

Figure 4 Indentation creep, at various experimental temperatures, in principal crystallographic directions on (a) the (001) plane and (b) the (111) plane.

duced in Fig. 5. The [110] indentations are invariably well formed with no surface or subsurface cracks. On the other hand, some cracks are observed in regions of intersecting slip lines around the [1$\bar{2}$1] indentations. Furthermore, the nature of deformation produced by indentations in these particular directions is not symmetrical. Note that the intersections of the slip traces with the (111) surface, shown in Fig. 5, are consistent with slip on {100} rather than {110} planes.

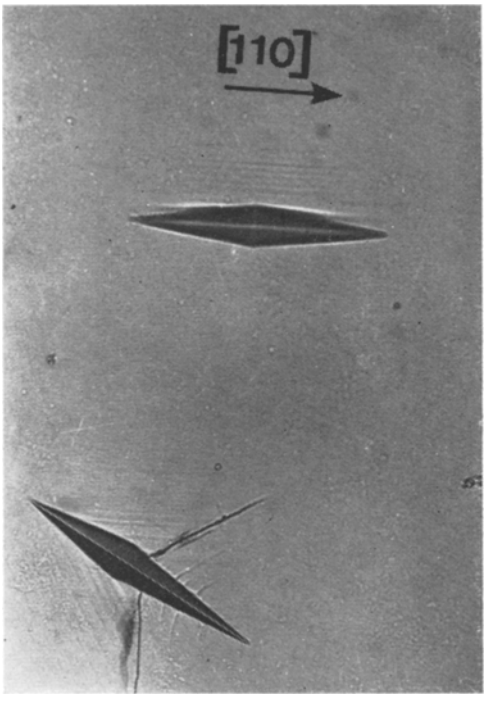

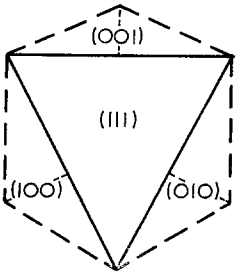

Figure 5 Knoop indentations on the (111) plane of calcium fluoride showing slip lines consistent with {001}⟨110⟩ systems. Also, note asymmetry of the deformation on each side of the long diagonal for the [1$\bar{1}$0] indentation and at each end of the [11$\bar{2}$] indentation. The three-fold symmetry of slip planes intersecting this surface contrasts with the two-fold symmetry of the indenter. (Unetched, × 1000.)

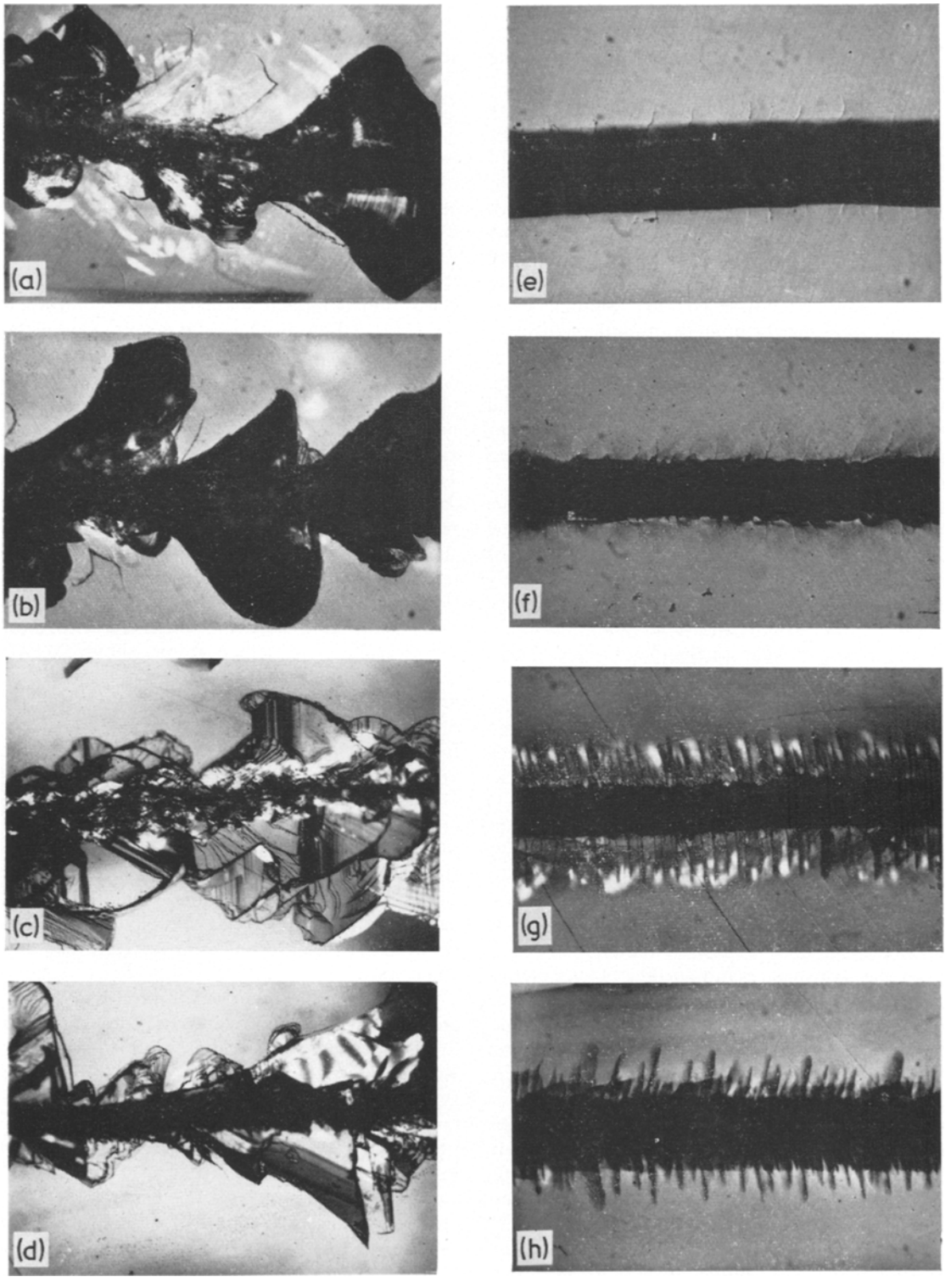

Figure 6 Typical wear tracks produced, by a 90° diamond cone and 300 g normal load, on calcium fluoride planes (a) [100] direction of sliding on (001) surface at 20°C. (Unetched, × 75.) (b) [110] direction of sliding on (001) surface at 20°C. (Unetched, × 75.) (c) $[11\bar{2}]$ direction of sliding on (111) surface at 20°C. (Unetched, × 50.) (d) $[\bar{1}\,\bar{1}2]$ direction of sliding on (111) surface at 20°C. (Unetched, × 50.) (e) [100] direction of sliding on (001) surface at 233°C. (Unetched, × 75.) (f) [110] direction of sliding on (001) surface at 233°C. (Unetched, × 75.) (g) $[11\bar{2}]$ direction of sliding on (111) surface at 253°C. (Unetched, × 50.) (h) $[\bar{1}\,\bar{1}2]$ direction of sliding on (111) surface at 253°C. (Unetched, × 50.)

Examples of the wear tracks produced in the [100] and [110] directions on the (001) plane of calcium fluoride, at room temperature, are shown in Fig. 6a and b. Surprisingly, cleavage fracture, which occurs readily on the {111} planes at room temperature under most conditions of deformation, is not an important part of the wear track formation on this plane. Any dislocation cracks which may have been formed during sliding are obliterated by the more catastrophic conchoidal fracture. Steijn [9] has reported a similarly limited amount of dislocation activity, at room temperature, very close to his friction tracks on calcium fluoride surfaces. He also observed a degree of conchoidal fracture which dominated the pattern of wear rather than fracture due either to dislocation interaction or cleavage.

Typical room temperature wear tracks in the $[11\bar{2}]$ and $[\bar{1}\bar{1}2]$ directions on the (111) plane are shown in Fig. 6c and d. The mechanisms of fragmentation on this plane are almost entirely dependent on fracture along the {111} cleavage planes rather than the conchoidal fracture characteristic of wear on the (001) plane. Again there is little evidence of cracking due to dislocation interactions. The sequence of crack formation for this (111) surface has been continuously observed, in this work, during the movement of a slider in the $[11\bar{2}]$ and $[\bar{1}\bar{1}2]$ directions. Sub-surface fractures, on the (111) cleavage plane, are invariably developed in front of the moving slider. These sub-surface cracks are bounded by fracture on certain of the {111} cleavage planes, i.e. planes of the type $(\bar{1}11)$ and $(1\bar{1}1)$, producing surface cracks on the (111) surface which are 30° to the direction of sliding. Both the sub-surface and surface cracks of this type are formed in front of the slider in that part of the material subjected to compressive stresses. Subsequently, as the slider passes over and between these initial cracks, further cracks are formed on the $(\bar{1}\bar{1}1)$ planes which intersect the surface normal to the direction of sliding. The wear fragments in the form of chevrons are finally detached when conchoidal fracture, developed by tensile stresses behind the slider, link up with the various cracks lying on {111} planes. The sequence of fragmentation in calcium fluoride is therefore similar in some ways to that previously observed at room temperature in magnesium oxide and lithium fluoride [2, 3]. The most significant difference is that the nature of fragmentation in calcium fluoride is predominantly determined by fracture on the {111} cleavage planes whilst in magnesium oxide and lithium fluoride it was principally due to fracture on {110} planes with limited fracture – under tensile stresses – on the {100} cleavage planes.

It is thought likely that the increase in the anisotropy of friction at higher temperatures is due to increased plastic deformation associated with the frictional process. Fig. 6e and f shows typical wear tracks on the (001) plane in the [100] and [110] directions at 233°C. Flow on the {100} ⟨011⟩ primary slip systems causes the build up of material along all ⟨110⟩ directions on the cube plane. Consequently, a slider has to plough through hills of displaced material whilst moving in the [110] directions but glides along valleys between these hills in the [100] direction. This effect is apparent in Fig. 6e and f. The two dark regions on each side of the [100] groove represent regions of material displaced by the slider in forming a valley. There is very little pile-up along the edges of the [110] groove because the slider is moving through and over the deformation hill. Very few cracks are formed on (001) surfaces at temperatures above 200°C. Sub-surface fractures are reduced in extent but are still evident beneath $[11\bar{2}]$ tracks formed at 253°C on the (111) cleavage surface. This type of fracture can be identified with the lighter regions around the groove shown in Fig. 6g. Both the $[11\bar{2}]$ and $[\bar{1}\bar{1}2]$ tracks produce cracks on the $(\bar{1}\bar{1}1)$ planes – i.e. those {111} planes which intersect the surface normal to the direction of sliding. A comparison of Fig. 6g with 6h also shows considerable slip line formation when sliding in $[11\bar{2}]$, due to flow on (010) [101] and (100) [011] systems, but comparatively little slip when sliding in $[\bar{1}\bar{1}2]$.

The distribution of dislocation etch pits, associated with indentations and friction tracks on {111} cleavage surfaces, is always consistent with plastic deformation on {001} ⟨110⟩ slip systems under all our particular experimental conditions.

5. Discussion

Compression and tension experiments on ceramic materials at room temperature have established that, under such experimental conditions, these materials are intrinsically brittle. However, it is also generally acknowledged that the stress distribution beneath an indenter or slider tends to inhibit brittle fracture and encourages dislocation mobility. Recent studies

on rutile [10], magnesium oxide [2, 3], aluminium oxide [11], transition metal carbides [12, 13] and even diamond [14, 15] have provided evidence of limited plastic flow during hardness and friction experiments. We now consider that plastic deformation is the controlling mechanism, rather than a secondary effect, and as such determines the nature of anisotropy in both hardness and friction measurements.

It is known that calcium fluoride cleaves on {1 1 1} planes. Also that the primary slip systems are {1 0 0} ⟨0 1̄ 1⟩ [6]. Identification of the slip systems has been determined in compression experiments where it was shown that slip on {1 0 0} and {1 1 0} occurred at temperatures above 60 and 200° C respectively. We shall show that significant plastic deformation can occur at room temperature, under our particular experimental conditions, on the primary slip systems and this determines the observed anisotropy.

5.1. Anisotropy in hardness

The indentation process, for a Knoop indenter, has recently been analysed and shown to be essentially determined by the crystal structure and the primary slip systems [4, 5]. A clear relationship between the mean effective resolved shear stress (τ'_e) and the observed hardness has been established for a wide range of crystalline solids. The effective resolved shear stress (τ_e) is calculated for each facet on the indenter using the following equation:

$$\tau_e = \frac{F}{A} \cos\phi \cos\lambda \left(\frac{\cos\psi + \sin\gamma}{2} \right) \quad (1)$$

where F = applied force; A = area supporting F; λ = angle between axis of F and slip direction ϕ = angle between axis of F and the normal to the slip plane; ψ = angle between the facet and the axis of rotation for a given slip system; γ = angle between the facet and the slip direction.

An arithmetic mean resolved shear stress (τ'_e) is then determined, for a specific indenter orientation, from the values of the maximum resolved shear stress developed by each of the four facets. Directions which correspond to the lowest values of τ'_e, for indentations on a given crystallographic surface, are found to be those of greatest hardness and the converse is also observed. The orientation of the deforming stress axis may be determined by either tensile or compressive forces which are parallel and normal to the indenter facets respectively. Generally, the nature of anisotropy indicated by Equation 1 is the same in both cases.

A detailed study of published results reveals that the only apparently anomalous results are obtained on {1 1 1} surfaces of face-centred cubic crystals and, as shown later in this work, fluorspar. Nevertheless, there is now sufficient experimental evidence to justify the use of this model to identify active slip systems in those crystals where it is possible for dislocations to move on more than one slip system. Consider the application of the analysis to calcium fluoride. Fig. 7a and b present the mean effective resolved shear stress curves for the {1 0 0} ⟨0 1 1⟩ and {1 1 0} ⟨1 1̄ 0⟩ systems respectively on the (0 0 1) plane. These curves indicate converse anisotropy for one set of slip systems compared with the other. Clearly, the hardness results shown in Fig. 1a and Fig. 2a imply that the {0 0 1} ⟨1 1 0⟩ slip systems control the indentation process in this crystal over the range from room temperature to 260° C. Any significant contribution from slip on the secondary {1 1 0} ⟨1 1̄ 0⟩ systems at elevated temperatures would reduce – or even reverse – the anisotropy. This effect has been observed in the behaviour of the transition metal carbides, of the rocksalt structure, where changes in the active primary slip system over a suitable range of experimental temperatures are reflected in the nature of anisotropy observed using the model based on the Knoop indenter [13]. Similar resolved shear stress curves for the (1 1 1) surface are shown in Fig. 6c. Solely on the basis of these curves, it would appear that the {1 1 0} ⟨1 1̄ 0⟩ slip systems govern the indentation process. However, this is not consistent with the observed slip line pattern around the indentations shown in Fig. 4 and the distribution of dislocations when the crystals were etched. There are two possible explanations. It has been shown that the Knoop model gives similar resolved shear stress curves, in the majority of cases, either for compressive stresses normal to the facets or tensile stresses parallel to them [5]. In this particular case only, the curve based on compressive stresses reflects the observed hardness values more accurately than those based on tensile stresses. An alternative explanation is that measurements with the Knoop indenter, which is essentially one of two-fold symmetry, do not truly reflect the anisotropy in hardness of a crystal plane which has three-fold symmetry. This explanation is supported by the particularly asymmetric deformation, shown in Fig. 5,

common to all indentations in the $\langle 11\bar{2} \rangle$ directions on the (111) plane. Clearly, that "half" of the indentation flanked by pronounced slip lines is shorter than that associated with the cracks. Similarly anomalous behaviour, without crack formation, has been observed only on (111) surfaces of fcc metals.

Fig. 4 indicates that the nature of anisotropy is not influenced by mechanisms of creep and relaxation underneath the indenter. These results can also be used to estimate the activation energy for the flow process [7, 16]. When two similar measurements are carried out at different temperatures (say T_1 and T_2) then, for a given hardness value, the displacement of the two straight line plots is given by:

$$\log_e t_1 - \log_e t_2 = \frac{Q}{R}\left(\frac{1}{T_1} - \frac{1}{T_2}\right) \qquad (2)$$

where t_1 and t_2 are the respective times for the two indentations at T_1 and T_2; Q is the activation energy for self-diffusion and R is the gas constant.

An activation energy of approximately 10 kcal mol^{-1} was calculated using Equation 2 and the results shown in Fig. 4. This is reasonably close to the value of 12.5 $\pm$ 0.8 kcal mol^{-1} reported for the vacancy diffusion of the F^- ion in calcium fluoride [17] and suggests that this is the mechanism controlling creep under these experimental conditions.

5.2. Anisotropy in friction

The frictional properties of nonmetallic crystals have been studied extensively during the last decade. Few explanations of anisotropy in friction have been based on adhesion. Buckley [18] suggested that the direction of minimum friction for sapphire was the direction of closest atomic packing on planes of greatest atomic density. He proposed that the adhesive junctions formed with such orientations are the easiest to shear but his experiments were based on measurements with comparatively low loads and metallic sliders which did not significantly deform the sapphire surface. His observation is not generally applicable to other nonmetallic crystals – particularly where appreciable penetration and deformation of the crystal surface by a harder slider is obtained. Childs [19] claimed that the anisotropy in friction of diamond cones on magnesium oxide surfaces was due to interfacial adhesion rather than to bulk deformation. However, the type of apparatus he used was unsuitable for studies of anisotropy since the slider was

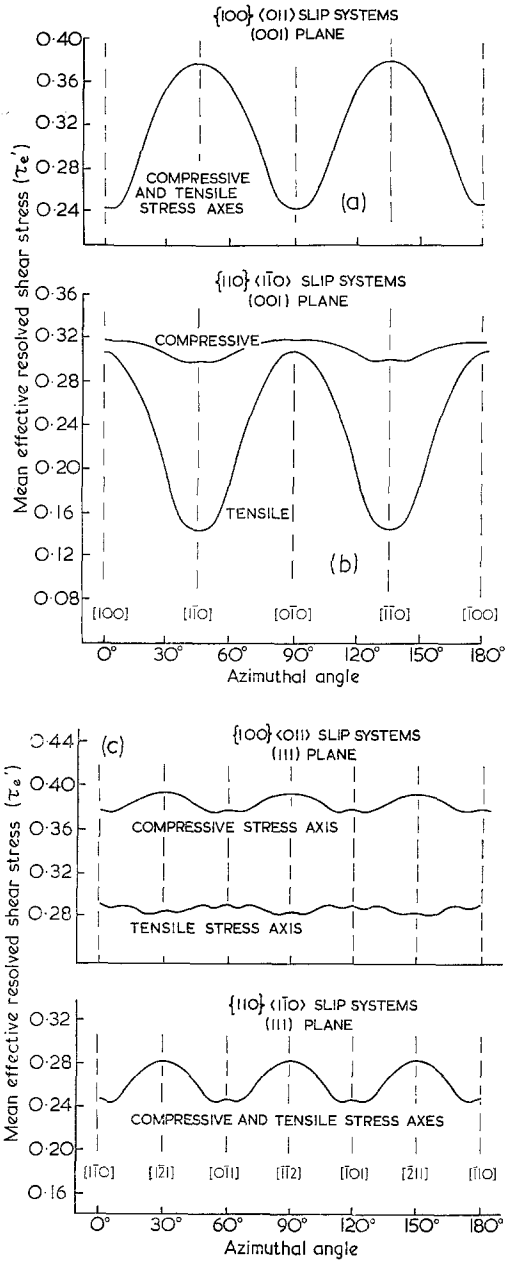

Figure 7 Distribution of the mean effective resolved shear stress in Knoop hardness measurements for (a) (001) plane, {001} ⟨110⟩ slip systems; (b) (001) plane, {110} ⟨1$\bar{1}$0⟩ slip systems; (c) (111) plane, {001} ⟨110⟩ slip systems and (111) plane, {110} ⟨1$\bar{1}$0⟩ slip systems.

mounted on a very flexible system and tended to produce a curved rather than a straight unidirectional track. The main reason given to support an adhesion mechanism was based simply on the observation that the degree of

anisotropy was reduced by the presence of a lubricant in conjunction with ultra-sonic vibrations. Apparently, no attempt was made to evaluate the effect of vibrations alone nor to analyse the possible effect of the ethyl alcohol "lubricant" on the nature and degree of associated plastic flow. In an earlier, and more convincing study, Buckley [20] had shown that the friction between a sapphire slider and a lithium fluoride crystal surface could be reduced by a solution which increased the extent of bulk and surface plastic deformation. Furthermore, recent work has confirmed that frictional measurements between diamond cones and magnesium oxide crystals can be directly influenced by bulk hardening mechanisms whilst the anisotropic properties are retained [4].

The majority of recent studies have increasingly emphasized the significance of plastic flow in the frictional deformation of some of the hardest and most brittle crystals. There is no complete model available, comparable with that developed for the Knoop indenter, to apply to frictional anisotropy in crystalline solids. However, Bowden and Brookes [2] explained the anisotropy they observed in magnesium oxide and lithium fluoride crystals on the basis of the differences in the magnitude and distribution of the resolved shear stresses during sliding in various crystallographic directions. They assumed that the axis of the normal load moves through the angle θ (where $\tan\theta = \mu$) in the direction of sliding. The resultant stress axis can then be used to determine the proportion of the applied stress resolved on the active slip systems, during sliding in a given crystallographic direction, from the equation:

$$\tau_f = \sigma \cos\alpha \cos\eta \qquad (3)$$

where τ_f is the resolved shear stress; σ the applied stress; α the angle between the resultant stress axis and the normal to the slip plane and η the angle between the resultant stress axis and the slip direction.

The relative distribution of the maximum resolved shear stresses in the bulk of a crystal, during sliding on a specific plane and in a given direction, can thus be determined even though their absolute magnitude cannot be predicted because the effective value of σ is not known. Clearly, this type of analysis assumes a radical simplification of the complex stress distribution in front of the sliding cone and must have limited applications. Nevertheless, this approach has been successfully applied to predict anisotropy on the (1 1 0) planes of magnesium oxide and lithium fluoride [2, 3].

If bulk deformation in calcium fluoride is controlled by $\{1\,1\,0\}\langle 1\bar{1}0\rangle$ slip systems, during friction measurements, the anisotropy would be the same as magnesium oxide and lithium fluoride – i.e. maximum and minimum values of μ on (0 0 1) surfaces in [1 0 0] and [1 1 0] directions respectively. Table I confirms that the reverse of this anisotropy is observed. We shall therefore consider the extension of a similar analysis to our results for calcium fluoride on the assumption that $\{0\,0\,1\}\langle 1\,1\,0\rangle$ are the primary slip systems.

Consider friction on the (0 0 1) plane of calcium fluoride. The relevant distribution of the resolved shear stresses for sliding in the [1 0 0] and [1 1 0] directions, using Equation 3, is shown in Fig. 8a and b respectively. The maximum shear stresses during sliding in the [1 0 0] direction are borne equally on four out of the possible six slip systems. These active systems are those based on the (0 0 1) planes parallel to the sliding surface and those (1 0 0) planes which intersect the surface normal to the friction track. The shear stress on the (0 1 0) planes is zero. On the other hand, the maximum resolved shear stresses for [1 1 0] sliding are restricted to one system – i.e. the (0 0 1) $[1\bar{1}0]$ – and are greater than for [1 0 0] sliding. Consequently, the application of a tangential force in the [1 1 0] direction causes greater penetration of the cone than in the [1 0 0] direction with a corresponding increase in the coefficient of friction. The degree of frictional anisotropy may well be increased by the formation of a "hill" of plastically deformed material directly in front of the cone before sliding in the [1 1 0] directions as observed in copper [21]. This effect would be emphasized when plastic deformation is facilitated at higher experimental temperatures and might account for the increased degree of anisotropy evident in Table I.

The situation is somewhat more complicated for friction on the (1 1 1) planes of calcium fluoride. The maximum resolved shear stress curves for sliding in the $[11\bar{2}]$ and $[\bar{1}\bar{1}2]$ directions on this plane are shown in Fig. 8c and d. There is clearly a significant difference in the distribution of the important resolved shear stresses for sliding in the opposite senses of this the same type of crystallographic direction. Sliding in the $[11\bar{2}]$ sense gives a maximum resolved shear stress on the two primary slip

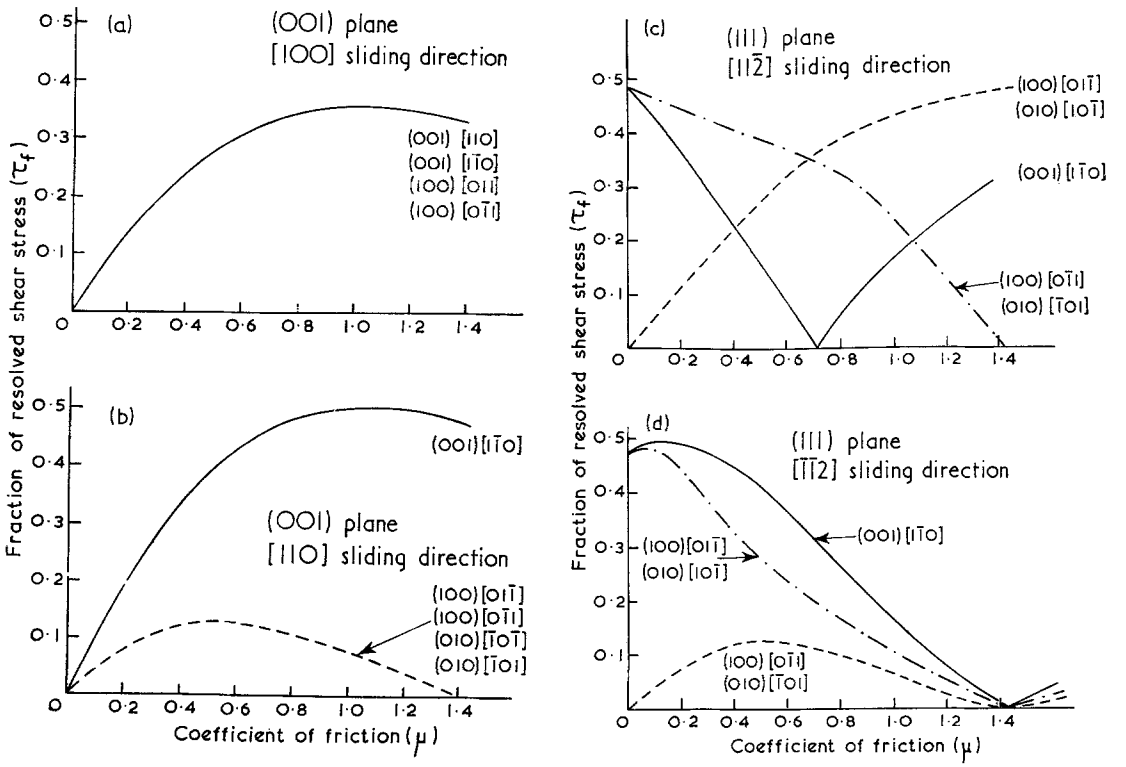

Figure 8 Distribution of resolved shear stresses, based on Equation 2 and {001} ⟨110⟩ slip systems, for friction measurements (a) [100] direction of sliding on (001) plane. Slip equal on (010) and (100) planes; (b) [110] direction of sliding on (001) plane. Slip predominant on (001) plane; (c) [11$\bar{2}$] direction of sliding on (111) plane. Slip equal on (010) and (100) planes; (d) [$\bar{1}\bar{1}$2] direction of sliding on (111) plane. Slip predominant on (001) plane.

planes, i.e. (010) and (100), which produces slip steps intersecting the surface at 30° to the wear track. In the {100} slip planes, only the (001) is activated by the maximum resolved shear stresses when sliding in the [$\bar{1}\bar{1}$2] sense. This produces slip lines which intersect the surface normal to the wear track. Evidence to support these explanations has previously been given in the description of the slip lines for each case and is apparent in Fig. 6g and h. Again we observe greater penetration, and a higher friction, when sliding in the direction with the fewest number of active slip systems – that is the [$\bar{1}\bar{1}$2]. Also, the crystallographically dependent pile-up of material can serve to increase the degree of anisotropy in a similar way to that suggested for the (001) plane. On the (111) plane, the hills are formed directly in front of the [$\bar{1}\bar{1}$2] track, the high friction direction, but on either side of the low friction [11$\bar{2}$] track.

An interesting point that arises from the resolved shear stress analysis is that these stresses tend to zero, for the {001} ⟨110⟩ slip systems, when sliding in the [$\bar{1}\bar{1}$2] direction with a value of $\mu = 1.4$. Therefore, we should expect a dramatic change in the deformation associated with this particular value of μ. Wear tracks were made in the [$\bar{1}\bar{1}$2] and [11$\bar{2}$] directions – on a (111) plane, using a 60° cone, a 1 kg normal load and an experimental temperature of 300°C – in order to investigate this possibility. Representative regions of these two wear tracks are reproduced in Fig. 9a and b. The [11$\bar{2}$] wear track has similar features to those made using a 90° cone with 300 g normal load at 253°C, shown in Fig. 6g, and indicates extensive plastic deformation with a slightly greater degree of associated fracture. However, there were significant differences in the corresponding [$\bar{1}\bar{1}$2] wear track. A groove of varying width was formed indicating severe pile-up ahead of the slider and, surprisingly at this temperature, extensive {111} cleavage fractures. The recorder trace for this case was also different from those made with blunter

cones and lighter loads. It was normally smooth for most of our measurements, indicating a reasonably constant value of μ, but this particular trace had a pronounced serrated form. Each drop in the value of the friction force corresponded to the formation of cleavage cracks.The variation in the friction forces from point to point gave rise to a range of μ between 0.95 and 1.45. This type of wear track can be explained by the following sequence. The slider is initially at rest in the material but pile-up occurs in front of the slider, as the applied tangential force is increased, making movement progressively more difficult. This pronounced pile-up is shown in the interferrogram of Fig. 9d. Ultimately, the tangential force will reach a value such that μ approaches 1.4. Further plastic deformation and pile-up is inhibited because the resolved shear stresses tend to zero on all the slip systems, and cleavage fractures develop. At this point, the slider momentarily jumps clear of the surface before repeating the initial process of pile-up.

5.3. Dislocation interactions

The absence of cracks due to dislocation interactions, during the hardness and friction experiments, is the most significant difference between the behaviour of calcium fluoride crystals and those of magnesium oxide and lithium fluoride [2]. This observation may be explained by considering the relevant interactions in a cubic crystal with $\{001\}\langle 110\rangle$ systems. There is only one such type of interaction which would reduce the overall elastic energy of the participating dislocations on these – the primary slip systems. This can be represented by the equation:

$$\tfrac{1}{2}a\,[01\bar{1}] + \tfrac{1}{2}a\,[101] \rightarrow \tfrac{1}{2}a\,[110]$$

The resultant dislocations with a Burgers vector of $\frac{1}{2}a\,[110]$ would lie on active slip planes, i.e. the (001), and would therefore not coalesce to initiate fracture. On the other hand, if any degree of dislocation activity was obtained on the $\{110\}\langle 1\bar{1}0\rangle$ slip systems then the following reaction is possible [22]:

$$\tfrac{1}{2}a\,[0\bar{1}1] + \tfrac{1}{2}a\,[10\bar{1}] \rightarrow \tfrac{1}{2}a\,[1\bar{1}0]$$

The dislocations produced by this reaction lie on $\{112\}$ planes and would thus be sessile. Subse-

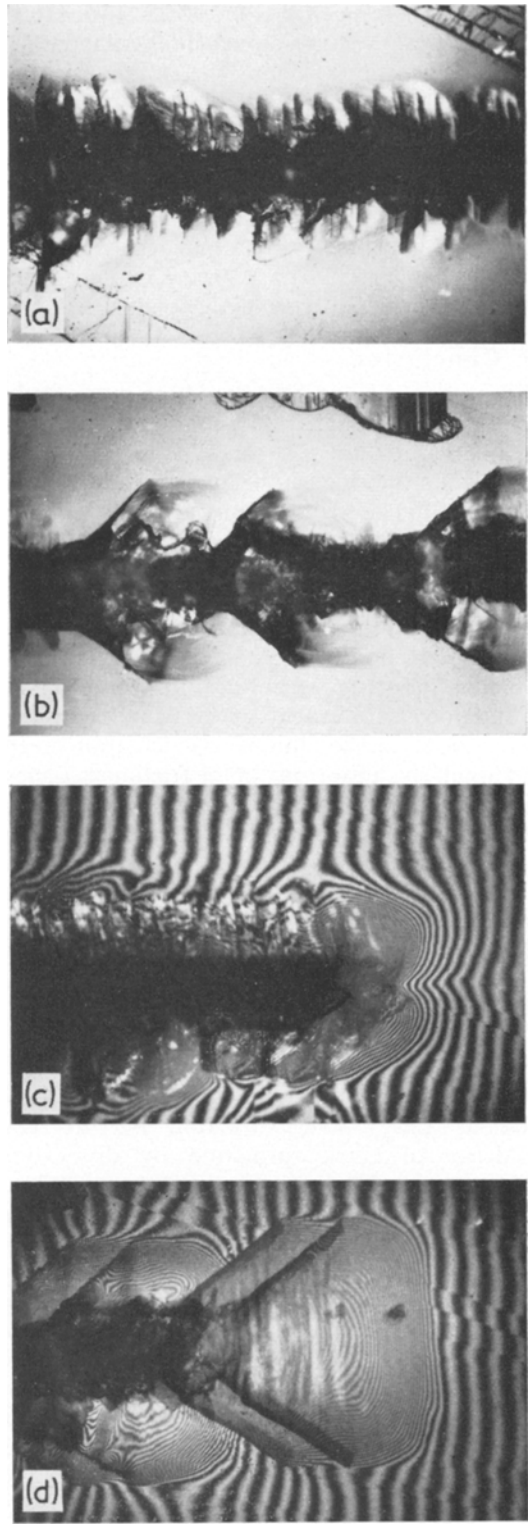

Figure 9 Wear tracks, produced by 60° cone and 1 kg normal load, on (111) surface at 300°C in (a) $[11\bar{2}]$ and (b) $[\bar{1}\bar{1}2]$ directions. Note the nature of pile-up to give valleys and hills respectively in the interferrograms of (c) $[11\bar{2}]$ and (d) $[\bar{1}\bar{1}2]$. (Unetched, × 50.

Figure 9

quent coalescence of the sessile dislocations would cause fracture along {110} planes. This reaction is the one responsible for the characteristic fracture observed in ionic crystals of the rocksalt type. Similar cracks were not observed in calcium fluoride crystals over the experimental temperature range covered in this work and this observation supports the contention that slip on {100} ⟨011⟩ systems predominates over that on the {110} ⟨1$\bar{1}$0⟩ systems during both hardness and friction measurements.

6. Conclusions

The principal points that have been made in this study may be summarized:

(i) Anisotropy in the hardness of (001) surfaces of calcium fluoride can be explained in terms of slip on {001} ⟨110⟩ systems using the effective resolved shear stress model developed in earlier work for a wide range of crystalline solids. The hardness results on {111} planes are apparently anomalous although similar results have also been obtained in fcc crystals on these particular planes. Anisotropy in hardness measurements is maintained at elevated experimental temperatures and under conditions of indentation creep.

(ii) Similarly, anisotropy in the frictional properties of calcium fluoride can best be explained on the basis of bulk plastic deformation due to slip on {001} ⟨110⟩ systems. It is possible that changes in surface topography, due to pile-up in specific crystallographic directions, emphasize the observed anisotropy. This is most likely at experimental temperatures in the range above 200°C where the grooves are formed predominantly by plastic deformation with comparatively little brittle fracture.

(iii) We have observed varying degrees of conchoidal and cleavage fracture but no real evidence of crack formation by dislocation interactions. However, dislocation etch pit distribution and slip lines consistent with flow on the {001} ⟨110⟩ primary slip systems have been observed. These observations, in conjunction with predictions based on resolved shear stress analyses, confirm that the anisotropy in hardness and friction is essentially controlled by mechanisms of bulk plastic deformation on {001} ⟨110⟩ slip systems in the temperature range 20 to 300°C.

Acknowledgements

We thank Professor D. L. Smare and the University of Bradford for a maintenance grant to one of us (J.B.O'N.), the SRC and UKAEA for research grants. We are also grateful to Professor H. G. Edmunds for his encouragement and Miss Jill Kent for technical assistance.

References

1. P R. BILLINGSHURST, C. A. BROOKES, and D. TABOR, *Proc. Phys. Soc.* (1966) 253.
2. F. P. BOWDEN and C. A. BROOKES, *Proc. Roy. Soc.* **A295** (1966) 244.
3. C. A. BROOKES and J. B. O'NEILL, Proc. Symp. Anisotropy in Refractory Compound Single Crystals, Vol. 2 (ed. F. W. Vahldiek and S. A. Mersol). (New York, Plenum Press, 1968) p. 291.
4. J. B. O'NEILL, Ph.D. Dissertation, University of Bradford, 1970.
5. C. A. BROOKES, J. B. O'NEILL, and B. A. W. REDFERN, *Proc. Roy. Soc.* **A322** (1971) 73.
6. A. G. EVANS, C. ROY, and P. L. PRATT, *Proc. Brit. Ceram. Soc.* **6** (1966) 173.
7. A. G. ATKINS, A. SILVERIO, and D. TABOR, *J. Inst. Metals* **94** (1966) 369.
8. M. BARQUIS, M. KENNEL, and R. COURTEL, *Wear* **11** (1962) 87.
9. R. P. STEIJN, *J. Appl. Phys.* **34** (1963) 419.
10. *Idem, ASLE Trans.* **12** (1969) 21.
11. B. J. HOCKEY, *J. Amer. Ceram. Soc.* **54** (1971) 223.
12. D. J. ROWCLIFFE and G. E. HOLLOX, *J. Mater. Sci.* **6** (1971) 1303.
13. R. J. HANNINK, D. KOHLSTEDT, and M. J. MURRAY, *Proc. Roy. Soc.* **A326** (1972) 409.
14. C. A. BROOKES, *Nature* **228** (1970) 660.
15. *Idem, Diamond Research* (1971) p. 12.
16. F. P. BOWDEN and D. TABOR, "Friction and Lubrication of Solids" (Clarendon Press, Oxford, 1964).
17. G. A. KEIG and R. L. COBLE, *J. Appl. Phys.* **39** (1968) 6090.
18. D. L. BUCKLEY, NASA TM X-52211 (1966).
19. T. H. C. CHILDS, *Wear* **13** (1969) 51.
20. D. L. BUCKLEY, NASA TM X-52211 (1966).
21. J. M. BAILEY and A. T. GWATHMEY, *ASLE Trans.* **5** (1962) 45.
22. A. S. KEH, C. H. LI, and Y. T. CHOU, *Acta Metallurgica* **7** (1959) 694.

Received 2 May and accepted 9 June 1972.